Classical and quantum mechanics of diatomic molecules in tilted fields

Carlos A. Arango, William W. Kennerly, and Gregory S. Ezra[a)]
Department of Chemistry and Chemical Biology, Baker Laboratory, Cornell University, Ithaca, New York 14853

(Received 31 January 2005; accepted 17 February 2005; published online 6 May 2005)

We investigate the classical and quantum mechanics of diatomic molecules in noncollinear (tilted) static electric and nonresonant linearly polarized laser fields. The classical diatomic in tilted fields is a nonintegrable system, and we study the phase space structure for physically relevant parameter regimes for the molecule KCl. While exhibiting low-energy (pendular) and high-energy (free-rotor) integrable limits, the rotor in tilted fields shows chaotic dynamics at intermediate energies, and the degree of classical chaos can be tuned by changing the tilt angle. We examine the quantum mechanics of rotors in tilted fields. Energy-level correlation diagrams are computed, and the presence of avoided crossings quantified by the study of nearest-neighbor spacing distributions as a function of energy and tilting angle. Finally, we examine the influence of classical periodic orbits on rotor wave functions. Many wave functions in the tilted field case are found to be highly nonseparable in spherical polar coordinates. Localization of wave functions in the vicinity of classical periodic orbits, both stable and unstable, is observed for many states. © *2005 American Institute of Physics*. [DOI: 10.1063/1.1888574]

I. INTRODUCTION

There has been considerable recent interest in the control of atomic and molecular quantum dynamics (see, for example Refs. 1–8 and references therein). Research on the control of molecular rotational degrees of freedom[9,10] includes production of specific states[11,12] or bands of highly excited rotational states,[13] rotationally induced bond dissociation,[13–17] and coherent control of periodically kicked molecules.[18–20] Particular attention has been given to the production of angularly localized (aligned or oriented) states.[2,4,9,21,22] For a recent survey, see Ref. 23.

In the present paper we consider the rotational dynamics of a diatomic molecule in a combination of strong static electric and pulsed nonresonant infrared laser fields. This combination of fields, primarily in the collinear configuration, has been investigated as a means of producing oriented states, both theoretically[24–27] and experimentally.[28–31] Here we study both the classical and the quantum mechanics for the case of tilted fields, where the classical dynamics is typically nonintegrable.[32] The properties of strongly mixed rotational quantum states produced by molecule-field interactions are a novel topic in the study of the classical-quantum correspondence for both integrable[33] and nonintegrable[34] systems. For example, both symmetric tops in static electric fields[35] and diatomics in collinear static and laser fields[36] exhibit quantum monodromy, a phenomenon recently studied in both atomic and molecular systems.[37–40] The classical phase space in the integrable collinear field case is organized by relative equilibria,[36] which are associated with stationary points of the effective angular potential.[41] Here we investigate the classical-quantum correspondence for the nonintegrable tilted field case, with special emphasis on the role of periodic orbits that evolve from the relative equilibria of the collinear field limit.

In Sec. II we provide some relevant background on the problem of rotational dynamics of molecules in strong external fields. The classical and quantum Hamiltonians for our system are introduced in Sec. III. Section IV presents our results on the classical phase space structure of the diatomic in collinear and tilted combined fields. In Sec. V we discuss our analysis of the nearest-neighbor level spacing distribution for the quantum problem, and correlate our findings with the corresponding classical dynamics. In Sec. VI we examine rotor wave functions, paying particular attention to localization of eigenfunction probability densities in the vicinity of classical periodic orbits. Section VII concludes.

II. ROTATIONAL DYNAMICS OF MOLECULES IN STRONG EXTERNAL FIELDS: GENERAL BACKGROUND

Beams of oriented molecules have long been used as probes of the orientation dependence of molecular collision dynamics.[2,21,42] Oriented states can be produced by "brute force" techniques, in which strong static uniform external E-fields induce mixing between J levels and lead to angular localization (nonzero $\langle P_1(\cos\theta)\rangle$).[21,43]

Field strengths used in brute force orientation require a nonperturbative approach to state mixing. For polar diatomics, the resulting oriented "pendular" states have received extensive study.[43–46] Some studies of state mixing in symmetric tops and asymmetric tops subject to intense external fields have also been carried out.[47,48] One focus of this work has been on the evolution of eigenstates from the zero field to the strong-field limit; sharply avoided crossings of energy

[a)]Electronic mail: gse1@cornell.edu

levels as a function of static field strength can lead to incorrect state labeling according to the zero-field limit parent in an adiabatic correlation scheme,[47] although in such cases it might be possible to provide physically significant labels in terms of diabatic states.

Onset of field-induced ionization limits experimental static electric-field strengths to values $\lesssim 5\times 10^4$ V cm^{-1}. This limitation on the static field strength has motivated the development of alternative approaches to producing angularly localized states for systems with small dipole moments and/or moments of inertia. Nonresonant linearly polarized laser fields oscillating at infrared frequencies lead, via second-order molecule-field interaction (mediated by molecular polarizability rather than dipole moment), to aligned states.[4,49–51] These pendular states have been investigated theoretically.[24,25,45,46,49]

An important aspect of the use of pulsed fields is the time dependence of alignment, both during[26,52–54] and following the pulse, so-called "field-free" alignment.[23] Studies of the quantal time evolution of rigid rotors subject to single nonresonant laser pulses have identified three regimes:[53] an adiabatic regime, where the pulse length $\tau_{\text{pulse}} \gg \tau_{\text{rot}}$, where τ_{rot} is the time scale for rotation; a short pulse regime, where $\tau_{\text{pulse}} \ll \tau_{\text{rot}}$; and an intermediate regime, where $\tau_{\text{pulse}} \sim \tau_{\text{rot}}$. In the adiabatic regime, the time dependence of the alignment essentially follows that of the nonresonant laser pulse.

For small enough values of angular momentum component m (see below), the effective potential in the coordinate θ (the angle between the diatomic axis and the laser polarization vector) associated with the nonresonant oscillatory field has the form of a double well, and closely spaced level doublets of aligned states are found at large field strengths.[25,49,51] Friedrich and Herschbach noted that application of a *collinear* static field leads to a splitting of the doublets, and so to the production of strongly oriented states.[24,25] This method for the production of oriented molecules has been verified experimentally for OCS molecules[28,29] (see also Ref. 30).

In the present study we focus our attention on the instantaneous rigid-rotor eigenstates in the combined static and laser fields, so that our considerations are relevant for the (experimentally accessible[28,29]) adiabatic regime.

A new level of complexity is attained by subjecting polar molecules to *tilted* static and oscillatory E-fields.[24] This case is now discussed in detail.

III. POLAR DIATOMIC MOLECULE IN TILTED FIELDS

In this section we consider the classical and quantum Hamiltonians for a diatomic molecule in combined static and nonresonant linearly polarized laser fields. In the general case, where the static field and laser field polarization vectors are not collinear, the classical problem is nonintegrable, and can exhibit complicated dynamics.

A. Classical mechanics

1. Hamiltonian

The classical Hamiltonian for a rigid polar diatomic in a static electric field ε_S along the space-fixed z axis is

$$H = H_0 - \varepsilon_S D\cos\theta = \frac{j^2}{2I} - \varepsilon_S D\cos\theta = \frac{1}{2I}\left[p_\theta^2 + \frac{p_\phi^2}{\sin^2\theta}\right] - \varepsilon_S D\cos\theta, \quad (1)$$

where j is the rotor angular momentum, I the moment of inertia, D the magnitude of the dipole moment, the spherical polar coordinates (θ,ϕ) describe the orientation of the rotor axis, and (p_θ, p_ϕ) are conjugate momenta. The angle between the diatom axis and the external field is θ. In terms of free-rotor action-angle variables (j,m,q_j,q_m),[55] $H=H(j,m,q_j)$ is a function only of j, m, and q_j,

$$H = \frac{j^2}{2I} - \varepsilon_S D\sqrt{1-\frac{m^2}{j^2}}\cos q_j. \quad (2)$$

The projection m (p_ϕ) is therefore a constant of the motion. The dependence of H on q_j results in j mixing (j is no longer a constant of the motion), while the dependence on m means that the angular momentum vector $\boldsymbol{j}$ precesses around the z axis with constant projection m.

Hamiltonians (1) and (2) describe the spherical pendulum.[33] The classical spherical pendulum, although an integrable system,[56] exhibits the phenomenon of *monodromy*, which is a topological obstruction to the existence of a global set of action-angle variables.[33] The quantum spherical pendulum exhibits *quantum monodromy*.[37] Eigenstates of the quantum spherical pendulum exhibit orientation of the rotor by the field.[43,45]

For a polarizable diatomic in a rapidly oscillating nonresonant (infrared frequency) linearly polarized laser field $\varepsilon_L(t)$ along the space-fixed z axis, the relevant Hamiltonian is the time-averaged interaction

$$H = \frac{j^2}{2I} - \frac{\langle\varepsilon_L(t)^2\rangle}{2}[\alpha_\perp + (\alpha_\parallel - \alpha_\perp)\cos^2\theta], \quad (3)$$

where $\alpha_\parallel, \alpha_\perp$ are components of the polarizability parallel and perpendicular to the diatomic axis, respectively, and $\langle\varepsilon_L(t)^2\rangle$ denotes the time-averaged laser field. If $\varepsilon_L(t) = f(t)\varepsilon_L\cos(2\pi\upsilon t)$, where υ is the laser frequency, ε_L the field amplitude, and $f(t)$ a slowly varying envelope function, then $\langle\varepsilon_L(t)^2\rangle = f^2\varepsilon_L^2/2$. Note that the molecule-field interaction depends on $\cos^2\theta$. The projection m is a constant of the motion, and the effective potential in the orientation angle θ has a double minimum (for small values of m^2). Quantum mechanically, for a strong field, extensive J mixing occurs to produce aligned rather than oriented states;[4,13,25,50] eigenstates of the double-well potential form closely spaced (parity) doublets.[25] Conservation of m means that the classical system is integrable. While there is no monodromy for the rotor in a linearly polarized laser field with no additional fields, the circularly polarized case does exhibit classical[33] and quantum[36] monodromy.

A more complicated but still integrable problem results when collinear static and linearly polarized laser fields are applied.[25] The effective potential in θ has (for small enough m) the form of an asymmetric double well.[25] In terms of dimensionless variables $\omega \equiv \varepsilon_S D/B$ and $\Delta\omega \equiv \langle \varepsilon_L(t)^2 \rangle (\alpha_\parallel - \alpha_\perp)/2B$ ($B \equiv \hbar^2/2I$), and omitting a constant energy shift, the scaled Hamiltonian $\tilde{H} \equiv H/B$ is

$$\tilde{H} = j^2 - \omega \cos\theta - \Delta\omega \cos^2\theta = \left[p_\theta^2 + \frac{p_\phi^2}{\sin^2\theta} \right] - \omega \cos\theta - \Delta\omega \cos^2\theta, \tag{4}$$

where $\omega \cos\theta$ is the static field term, $\Delta\omega \cos^2\theta$ is the term due to the laser field, and j is now a dimensionless angular momentum measured in units of $\hbar$. The larger the parameter $\Delta\omega$, the greater the number of aligned states trapped in the double well; the larger the value of ω, the more asymmetric the well. The classical dynamics depends only on the dimensionless ratio $\mathcal{A} \equiv \omega/\Delta\omega$, whereas the quantum problem depends also on the magnitude of $\hbar$ through the rotational energy $B\hbar^2$. The quadratic spherical pendulum Hamiltonian (4) shows classical and quantum monodromy.[36,40,57]

A weak static field desymmetrizes the laser field potential and leads to a splitting of the parity doublets found in the absence of the static field. The eigenstates can then exhibit *orientation* enhanced over the value obtainable with the static field only.[25,51]

The dynamics becomes more complex when the static and laser field directions are tilted with respect to one another.[24,25,36] Setting the static field ε_S along the direction $(\sin\beta, 0, \cos\beta)$ in the xz plane, the scaled classical Hamiltonian is

$$\tilde{H} = j^2 - \omega[\sin\beta \sin\theta \cos\phi + \cos\beta \cos\theta] - \Delta\omega \cos^2\theta, \tag{5}$$

and is a function of all four free-rotor action-angle variables

$$\tilde{H} = j^2 - \omega \left\{ \sin\beta \left[-\left(\frac{m}{j}\right) \cos q_m \cos q_j - \sin q_m \sin q_j \right] + \cos\beta \sqrt{1 - \frac{m^2}{j^2}} \cos q_j \right\} - \Delta\omega \left[1 - \frac{m^2}{j^2} \right] \cos^2 q_j. \tag{6}$$

The "downright botanical" complexity of the quantum eigenstates previously noted in the tilted field case[25] is a consequence of classical *nonintegrability*.[32] The classical Hamiltonian (6) for the tilted field case no longer conserves m and there is both j and m mixing, so that the classical motion can exhibit chaos. The complicated classical dynamics arises from a competition between the tendency of the rotor to align along the laser field axis and the tendency to orient along the static field. Quantum mechanically, the presence of the $\cos\phi$ term in Hamiltonian (5) leads to M mixing as well as J mixing. We shall investigate numerically both the classical and quantum mechanics for a rigid diatomic in tilted fields, Eq. (5).

The model parameters we use are appropriate for the diatomic KCl (cf. Table III of Ref. 25): $B = 0.1286\ \text{cm}^{-1}$, $\mu = 10.48$ D, $\Delta\alpha \simeq 3.1\ \text{Å}^3$, so that $\omega = 41.1$ for $\varepsilon_S = 30\ \text{kV cm}^{-1}$ and $\Delta\omega = 240$ for $\varepsilon_L = 10^{12}\ \text{W cm}^{-2}$. For KCl we therefore have $\Delta\omega \lesssim 240$ and $\omega \lesssim 50$ for experimentally attainable field strengths, so that the number of trapped pendular states created by both the static field and the laser pulse for reasonable intensities is large enough for semiclassical considerations to be appropriate (that is, $\omega, \Delta\omega \gg 1$). Moreover, in this semiclassical regime the dimensionless ratio $\mathcal{A} \equiv \omega/\Delta\omega$ of the static field interaction energy to the laser field interaction energy can be in the range $1/6 - 1/4$, where significant classical chaos is present for large tilt angles (see below).

Other molecules for which the dynamical regime investigated here could be realized experimentally are bimetallic compounds LiM.[58]

2. Classical trajectories and surfaces of section

To avoid singularities in the classical equations of motion for the rotor expressed either in terms of spherical polar coordinates $(\theta, \phi, p_\theta, p_\phi)$ (5) or free-rotor action-angle variables (j, m, q_j, q_m) (6), we integrate trajectories using Cartesian coordinates (x, y, z) and associated conjugate momenta (p_x, p_y, p_z). The holonomic constraint of constant bond length, $x^2 + y^2 + z^2 = \text{const}$, is imposed via a Lagrangian multiplier.[59] This constraint can easily be relaxed to allow bond stretching and dissociation. Integration of trajectories is performed using a sixth-order hybrid Gear algorithm.[60]

At any time step along the trajectory, we can extract values of either spherical polar coordinates and their conjugate momenta or of free-rotor action-angle variables, together with the time derivatives of all these quantities. Details of the transformations involved are given elsewhere.[61]

The phase space for the diatomic rotor in tilted fields is four dimensional. In the collinear field case ($\beta = 0$) the existence of two constants of the motion E and m means that the phase space explored by a typical trajectory is two dimensional. In the general tilted field case, however, when $\beta \neq 0$, the only constant of the motion is the total energy and motion can occur on a three-dimensional manifold as well as on two-tori and periodic orbits.

We use Poincaré surfaces of section[32] (SOS) to explore the classical phase-space structure as a function of energy and other parameters. Surfaces $\Sigma(\boldsymbol{z})$ are defined by the condition $q_i = \text{const}$, where q_i is a canonical variable. Values of the other conjugate pair of variables (q_j, p_j) are recorded every time a trajectory crosses Σ with $\dot{q}_i > 0$.

3. Involutions, lines of symmetry, and periodic solutions

Hamilton's equations of motion (5) are invariant under the change of variables S,

$$S: (t, \theta, \phi, p_\theta, p_\phi) \mapsto (-t, \theta, 2\pi - \phi, -p_\theta, p_\phi). \tag{7}$$

The transformation S is an involution (self-inverse operation)

$$SS = I, \tag{8}$$

where I is the identity transformation. If P^{-1} is the inverse of the Poincaré map P, then the product $P^{-1}S$ is also an invo-

lution, and P can be written as the product of two involutions,[32,62]

$$P = S(P^{-1}S). \tag{9}$$

A *symmetry line* L_σ on a given SOS is the intersection of the SOS with the set of phase points invariant under the involution σ. For $\sigma=S$, the symmetry line on the (θ, p_θ) SOS defined by $\phi=0$ or π, $\dot{\phi}>0$, is the line $p_\theta=0$. Periodic solutions lying on symmetry lines can be found efficiently by locating the intersections of the symmetry line with its iterates under the map P.[62] Any phase point lying on such an intersection after a single iteration is either a period-1 or a period-2 periodic orbit.

Analysis of the iterated symmetry line L_S is performed in Cartesian coordinates. A one-parameter family of rotor phase points on L_S at fixed energy is defined by the conditions $y=0$, $\dot{z}=0$, $\dot{x}=0$, $\dot{y}>0$. Both positive and negative values of x are allowed, so that the $(\phi=0, \dot{\phi}>0)$ and $(\phi=\pi, \dot{\phi}<0)$ surfaces of sections are treated together. Each point in this family of initial conditions is propagated forwards in time until its trajectory intersects the xz plane $(y=0)$ again in the positive sense $(\dot{y}>0)$. Since $\dot{x}\propto\dot{z}$ for phase points in the xz plane (except at the poles!), those phase points having $\dot{z}=0$ again lie on the symmetry line L_S. These points can therefore be found by one-dimensional interpolation.

B. Quantum mechanics

1. Eigenvalues and eigenvectors

Eigenvalues and eigenvectors for the quantum version of Hamiltonian (4) are computed by matrix diagonalization in a basis of spherical harmonics $Y_M^J(\theta,\phi)$. Our computer program allows for nonconservation of the quantum number M, as required for the tilted fields case. For the tilting angle $\beta\neq 0$, eigenfunctions ψ_ν of the quantum Hamiltonian are superpositions

$$\psi_\nu = \sum_{J,M} c_{\nu,JM} Y_M^J(\theta,\phi). \tag{10}$$

Standard checks are carried out for convergence of the computed levels with respect to basis size.[63] In the following, probability densities $\rho(\theta,\phi)=\sin\theta|\psi_\nu(\theta,\phi)|^2$ associated with eigenstates (10) are plotted, and patterns of wave-function localization in the vicinity of classical periodic orbits (scarring[64]) are investigated.

For $0<\beta<\pi/2$, the only symmetry of the Hamiltonian is the reflection operation σ_{xz}, with associated angle transformation $\sigma_{xz}:(\theta,\phi)\mapsto(\theta,-\phi)$. A suitably symmetrized basis is then

$$|J,|M|,\pm\rangle = \frac{1}{\sqrt{2}}[Y_{|M|}^J \pm (-)^M Y_{-|M|}^J], \quad 1\leq|M|\leq J, \tag{11}$$

with $|J,0,+\rangle \equiv Y_{M=0}^J$. For $\beta=\pi/2$, the Hamiltonian is in addition invariant under reflection σ_{yz} and rotation C_{2x}.

The quantum calculations of energy levels used for the analysis of nearest-neighbor level spacing statistics given below are carried out in the symmetrized basis and the positive-parity $(+)$ state level statistics analyzed.

IV. CLASSICAL DYNAMICS AND PHASE-SPACE STRUCTURE

In this section we investigate the classical phase space of the rotor in collinear and tilted fields. We identify key structures in phase space (low-order stable and unstable periodic orbits, resonance islands, and regions of chaotic motion) and study their dependence on Hamiltonian parameters. We do not provide a comprehensive survey of the classical dynamics, but rather briefly describe those classical phase space features that are important for understanding and interpreting the properties of the corresponding quantum system. More details on the classical dynamics can be found in Ref. 61.

The classical mechanical problem is integrable for collinear fields ($\beta=0$). Our classical trajectory survey shows the existence of a significant fraction of chaotic classical phase space for ratios $\mathcal{A}\gtrsim 0.25$ and tilt angles $\beta\sim\pi/4$ (see below).

A. Diatomic rotor in collinear fields: Integrable dynamics

For the diatomic molecule in collinear static and laser fields ($\beta=0$), with scaled Hamiltonian (4), ϕ is an ignorable coordinate and $p_\phi=m$ is a constant of the motion, as is $\tilde{H}$ itself. The static field case ($\Delta\omega=0$) is the well-known spherical pendulum problem.[33,56,65] A more extensive discussion of the classical mechanics of the rotor in the pulsed laser field ($\omega=0$) is given in Ref. 61. Here we mainly focus on the physically and dynamically interesting ratio $\mathcal{A}=\omega/\Delta\omega=1/4$.

The effective potential $V_{\rm eff}(\theta;m)$ for θ motion at fixed m is

$$V_{\rm eff}(\theta;m) = \frac{m^2}{\sin^2\theta} - \omega\cos\theta - \Delta\omega\cos^2\theta. \tag{12}$$

Effective potentials for several different values of $m^2/\Delta\omega$ are shown in Figs. 1(a) ($\mathcal{A}=0$) and 1(b) ($\mathcal{A}=1/4$), respectively. Classical *relative equilibria*[41] correspond to critical points of $V_{\rm eff}$,

$$\frac{\partial V_{\rm eff}}{\partial\theta} = 0. \tag{13}$$

Scaled energies $\bar{E}\equiv\tilde{E}/\Delta\omega$ vs θ values for relative equilibria are shown in Fig. 1. Consider first the case with $\mathcal{A}=0$, $\Delta\omega>0$ (laser field only), Fig. 1(a). At energies just above $E=0$ there are three curves, associated with the two symmetrically located potential minima and a central potential maximum. The lowest-energy point on each of the three curves is a relative equilibrium with $m=0$. The two stable relative equilibria with $m=0$ correspond to the rotor stationary either parallel $(\theta=0)$ or antiparallel $(\theta=\pi)$ to the field; the unstable relative equilibrium at $\theta=\pi/2$ corresponds to a one-parameter family of stationary rotor configurations in the full phase space, parametrized by azimuthal angle $\phi=\phi_0$. For $|m|>0$, the relative equilibria are associated with pairs of periodic orbits with $\pm m$ (conical pendulum orbits[66]). The relative equilibria merge at $E=\Delta\omega$ in a symmetric pitchfork bifurcation, a consequence of the invariance of $V_{\rm eff}$ under the transformation $\theta\rightarrow\pi-\theta$ of $V_{\rm eff}$.

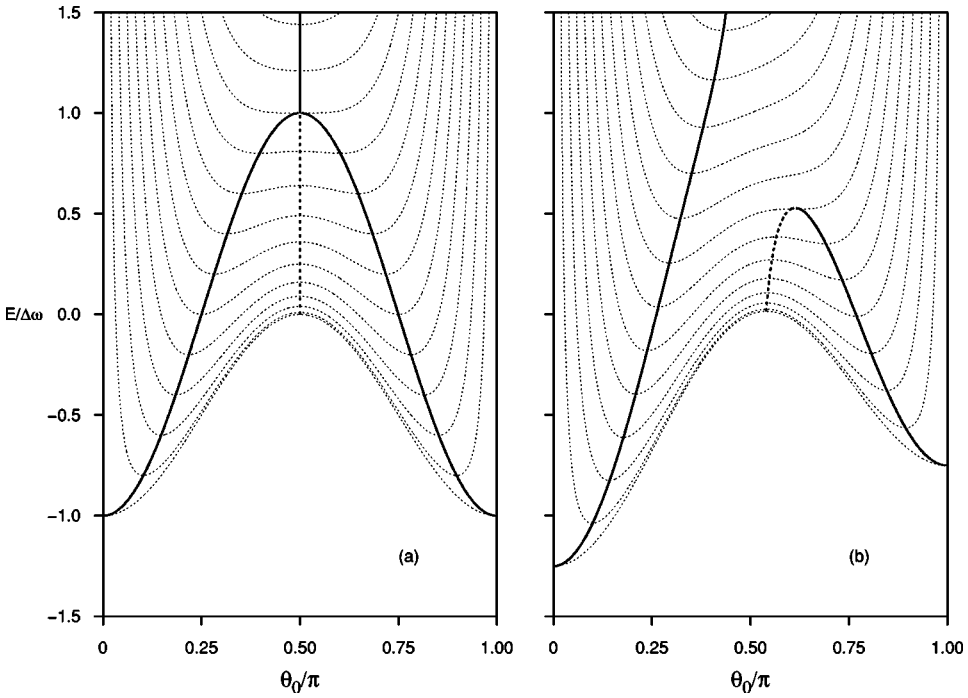

FIG. 1. Effective potential V_{eff} for different values of $m^2/2I\Delta\omega$, $\Delta\omega>0$ [see Eq. (12)]. (a) $\omega/\Delta\omega=0$. (b) $\omega/\Delta\omega=1/4$.

Relative equilibria for $\mathcal{A}=1/4$ are shown in Fig. 1(b) and, together with other periodic orbits, in Fig. 2(a). The symmetry $\theta\rightarrow\pi-\theta$ is now broken, and one of the stable relative equilibrium periodic orbit pairs merges with the unstable relative equilibrium orbit pair in a pair of saddle-node bifurcations.[67] In addition to the relative equilibria, there also exist one-parameter families of planar ($m=0$) periodic orbits passing through the poles. These orbits are librational (pendular) for energies below the barrier height, and rotational at higher energies. The transition from librational to rotational motion occurs at precisely the energy at which the unstable relative equilibrium appears. These additional orbits are represented by vertical traces at $\theta=0$ and π in Fig. 2(a) [cf. Fig. 3(b)]. Also shown in Fig. 2(a) are 1:1 resonant parabolic (neutrally stable) periodic orbits that emerge from the planar polar orbits and merge with the relative equilibria (conical pendulum orbits) at higher energy. These resonant periodic orbits occur in one-parameter families, with each family filling a rational torus. Particular orbits in the family are found by iteration of the symmetry line $p_\theta=0$ on the $\phi=0$, $\dot{\phi}>0$ surface of section (cf. Sec. III A 3).[62] The extra lines in Fig. 2(a) show the θ values for 1:1 resonant periodic orbits on the symmetry line at energy E. Each resonant torus intersects the symmetry line at two points, one on each side of a stable

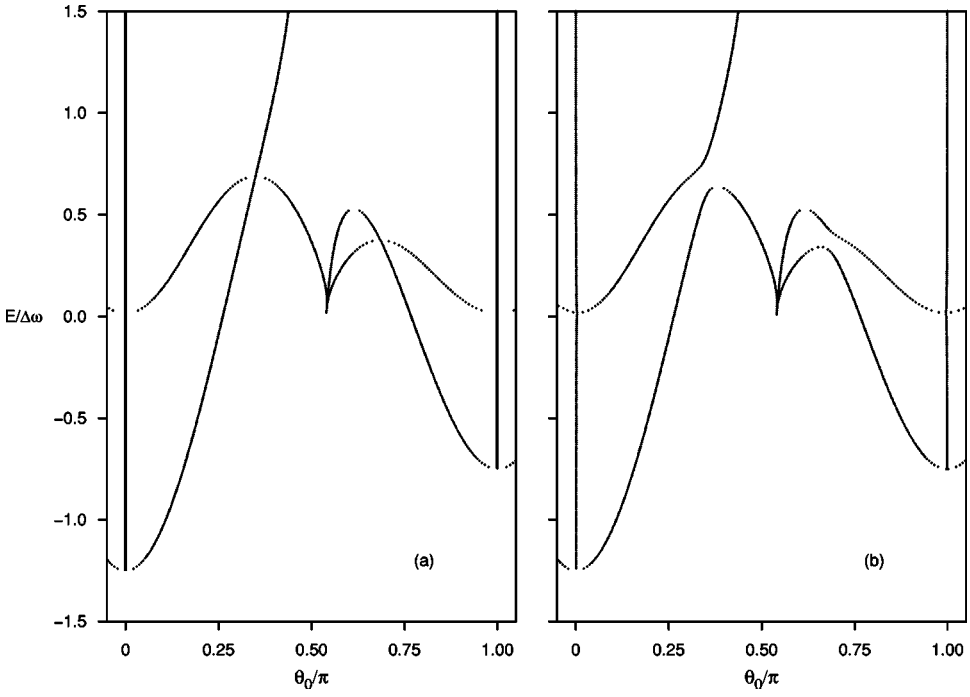

FIG. 2. Bifurcation diagrams showing E vs θ for relative equilibria and resonant periodic orbits in combined static and linearly polarized laser fields, $\omega/\Delta\omega=1/4$. (a) Collinear fields, $\beta=0$. (b) Tilted fields with small tilting angle, $\beta=0.01\pi$.

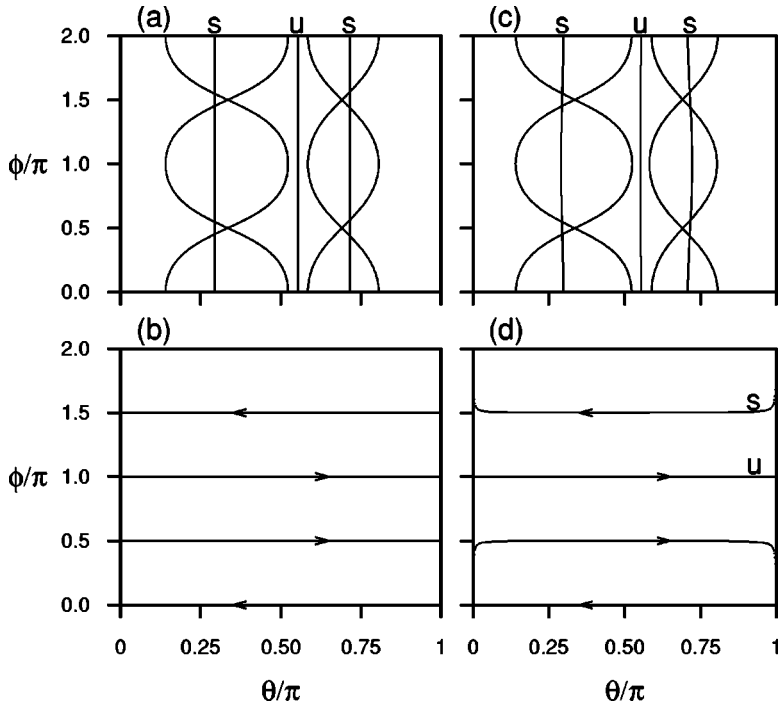

FIG. 3. Periodic orbits for $E=0.25$, $\omega/\Delta\omega=1/4$. (a) Collinear fields, $\beta=0$. Stable and unstable conical pendulum orbits (relative equilibria) are shown, together with 1:1 resonant periodic orbits. (b) Collinear fields, $\beta=0$. Two marginally stable planar periodic orbits passing through the poles are shown. (c) Tilted fields with small tilting angle, $\beta=0.01\pi$. Deformed conical pendulum orbits and resonant periodic orbits are shown. (d) Tilted fields with small tilting angle, $\beta=0.01\pi$. Stable periodic orbit rotating around x axis and unstable periodic orbit in xz plane are shown.

relative equilibrium. Unlike the periodic orbits associated with the relative equilibria, the angle θ is not constant along the 1:1 resonant periodic orbits [see Fig. 3(a)].

The corresponding E vs m plot for the relative equilibria is the classical energy-momentum diagram.[33] Classical $E-m$ diagrams for collinear fields have been given in Ref. 36.

Contours of m^2 in the (p_θ,θ) plane for $\mathcal{A}=1/4$ at fixed $\overline{E}$ are shown in Fig. 4(a) ($\overline{E}=1$) and 4(c) ($\overline{E}=0.2$). At the higher energy there is only a single stable equilibrium point (above the energy of the saddle-center bifurcation) while at the lower energy there are two stable and one unstable equilibrium points (below the saddle-center bifurcation). We define a (θ,p_θ) surface of section by conditions $\phi=0$ (or π) and $\dot{\phi}>0$. The invariant curves in the (θ,p_θ) SOS for $\overline{E}=1.0$ [Fig. 4(b)] and $\overline{E}=0.2$ [Fig. 4(d)] coincide with contours of m^2 for the same parameter values, thus confirming the cor-

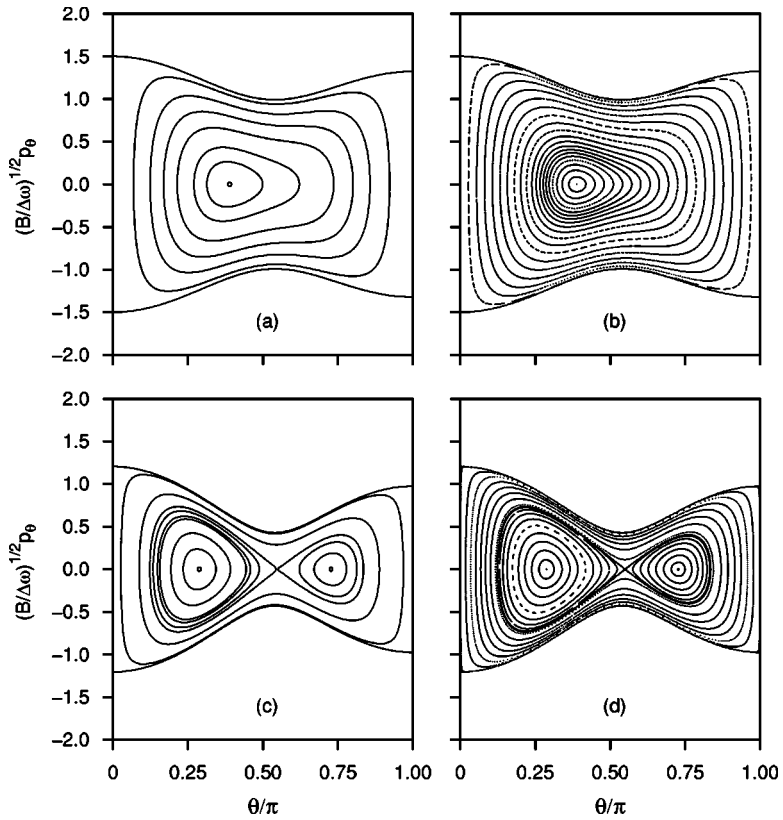

FIG. 4. (a) (θ,p_θ) reduced phase space, $\omega/\Delta\omega=1/4$, $E=1$. There is only one stable fixed point. (b) (θ,p_θ) surface of section, $\phi=0$, $\dot{\phi}>0$. $\omega/\Delta\omega=1/4$, $E=1$. (c) $\theta-p_\theta$ reduced phase space, $\omega/\Delta\omega=0.25$ and $E=0.2$. There are two stable fixed points and one unstable fixed point. The separatrix curve delimits the different types of motion (pendular and free rotor). (d) (θ,p_θ) surface of section, $\phi=0$, $\dot{\phi}>0$. $\omega/\Delta\omega=1/4$, $E=0.2$.

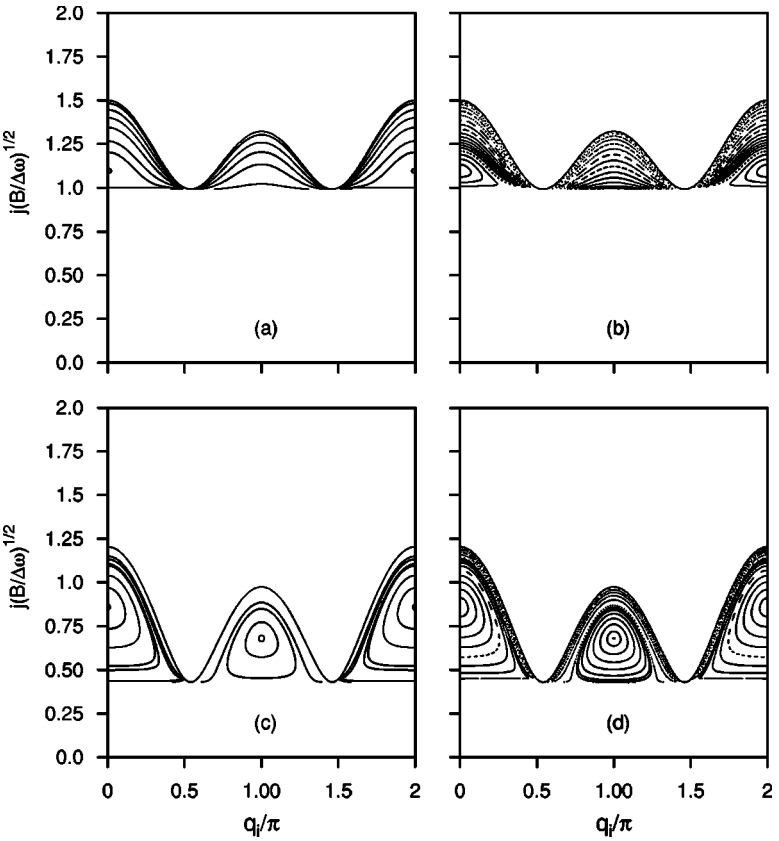

FIG. 5. (a) (j,q_j) reduced phase space, $\omega/\Delta\omega=1/4$, $E=1$. (b) (j,q_j) surface of section, $q_m=0$, $\dot{q}_m>0$. $\omega/\Delta\omega=1/4$, $E=1$. (c) (j,q_j) reduced phase space, $\omega/\Delta\omega=0.25$ and $E=0.2$. There are two stable fixed points and one unstable fixed point. The separatrix curve delimits the different types of motion (pendular and free rotor). (d) (j,q_j) surface of section, $q_m=0$, $\dot{q}_m>0$. $\omega/\Delta\omega=1/4$, $E=0.2$.

rectness of our trajectory numerics and the associated transformations from Cartesian to polar coordinates.

It is also interesting to examine the classical dynamics in free-rotor action-angle variables (j,m,q_j,q_m),[55] in terms of which the Hamiltonian is [setting $\beta=0$ in Eq. (5)]

$$\tilde{H}(q_j,j,m) = j^2 - \omega\sqrt{1-\frac{m^2}{j^2}}\cos q_j - \Delta\omega\left(1-\frac{m^2}{j^2}\right)\cos^2 q_j. \tag{14}$$

Rearranging to get m^2 as a function of q_j, j^2, q_j, and $\bar{E} \equiv \tilde{E}/\Delta\omega$ gives

$$m^2 = j^2\left\{1-\frac{1}{4\cos^2 q_j}\left[-\mathcal{A}\pm\sqrt{\mathcal{A}^2-4\bar{E}+\frac{4j^2}{\Delta\omega}}\right]^2\right\}. \tag{15}$$

There are two possible solutions corresponding to $\pm$ signs. Since we must have $\sin\theta \geqslant 0$, the physically relevant range of q_j for the first branch (positive sign) is $3\pi/2 \leqslant q_j \leqslant \pi/2$ (mod 2π), while that for the second (negative sign) is $\pi/2 \leqslant q_j \leqslant 3\pi/2$.

Contours of m^2 are shown in Fig. 5(a) for the case $\bar{E}=1$, $\mathcal{A}=1/4$, as in Fig. 4(a). The stable fixed point appears at $q_j=0$ (mod 2π). Figure 5(c) shows contours of m^2 for $\bar{E}=0.25$. Corresponding SOSs in action-angle variables (j,q_j) defined by $q_m=0,\dot{q}_m>0$ are shown in Figs. 5(b) and 5(d), respectively. In the SOS of Fig. 5(b) there is only one fixed point, a stable po at $q_j=0$, corresponding to the single stable relative equilibrium at this energy. Some invariant curves are clearly associated with librations around $q_j=0$, while the rest correspond to rotations in q_j. In Fig. 5(d) there are two stable fixed points (relative equilibria), at $q_j=0$ and $q_j=\pi$. Around each of these stable pos there is an associated quasiperiodic region, the region around $q_j \simeq \pi$ corresponding to larger potential energy. The unstable relative equilibrium appears at $q_j=\pi/2,3\pi/2$. Again, comparison of m^2 contours with SOS shows that the transformation of coordinates along trajectories has been correctly implemented.

B. Diatomic rotor in tilted fields: Nonintegrable dynamics

We now turn to the tilted field case, $\beta\neq 0$. The angular momentum component m is no longer conserved, and the dynamics is no longer integrable. We shall examine several SOSs for fixed $\mathcal{A}=\omega/\Delta\omega=1/4$ as a function of energy $\bar{E}$ and the tilt angle β, with a focus on the most important low-order pos that evolve from relative equlibria in the collinear field case, and on the onset of localized and global chaos.

1. Small tilting angle

When the tilting angle $\beta\neq 0$ there are new features in the dynamics. The only global constant of the motion is the Hamiltonian

$$H(\theta,\phi,p_\theta,p_\phi) = \frac{1}{2I}\left(p_\theta^2+\frac{p_\phi^2}{\sin^2\theta}\right) - \omega(\sin\beta\sin\theta\cos\phi + \cos\beta\cos\theta) - \Delta\omega\cos^2\theta. \tag{16}$$

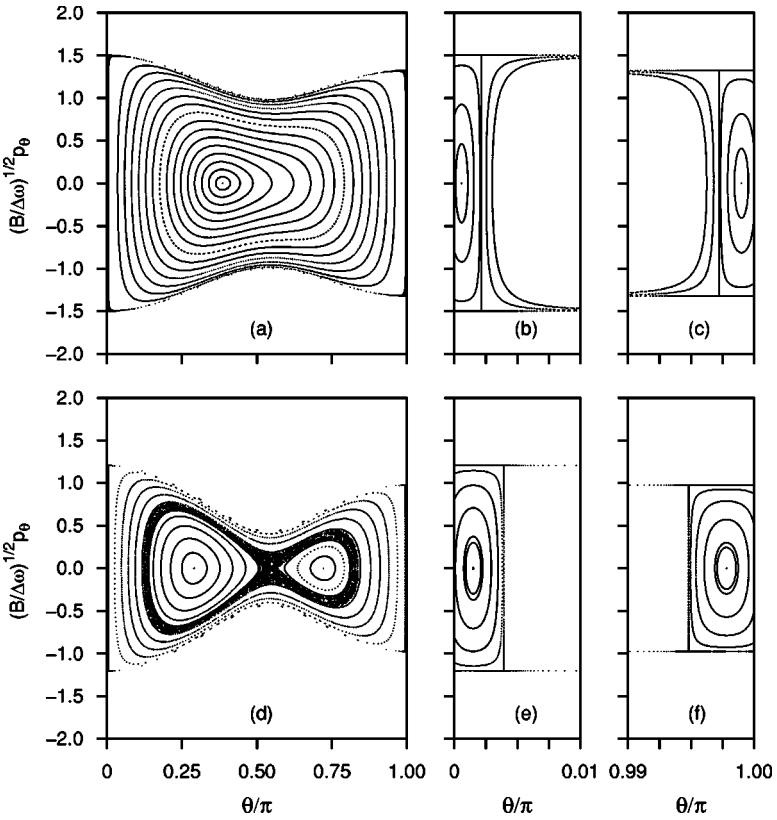

FIG. 6. (θ,p_θ) surfaces of section, defined by $\phi=0$, $\dot{\phi}>0$. $\omega/\Delta\omega=1/4$, $\beta=\pi/100$. (a) $E=1.0$. (b) $E=1.0$. Detail of the SOS near $\theta=0$. (c) $E=1.0$. Detail near $\theta=\pi$. (d) $E=0.2$.(e) $E=0.2$. Detail of the SOS near $\theta=0$. (f) $E=0.2$. Detail near $\theta=\pi$.

For $\beta=\pi/100$ and $\bar{E}=1.0$ the (θ,p_θ) SOS [Fig. 6(a)] is very similar in appearance to Fig. 4(b), except near $\theta=0$ and $\theta=\pi$. There are two new stable fixed points with $p_\theta=0$ close to $\theta=0$ and $\theta=\pi$, and Figs. 6(b) and 6(c) show these regions in detail. The stable fixed points of Fig. 6(b) and 6(c) correspond to clockwise and counterclockwise rotations, respectively, about the lab-fixed x axis in the yz plane. The (θ,p_θ) SOS for $\bar{E}=0.2$ is shown in Fig. 6(d). The conical pendulum periodic orbits (stable relative equilibria) for $\beta=0$ [Fig. 3(a)] are now deformed [Fig. 3(c)], although they remain stable. Although invisible on the scale of the figure there are two stable fixed points near $\theta=0$ and $\theta=\pi$ as for $\bar{E}=1$ [cf. Figs. 6(e) and 6(f)]. These stable fixed points again correspond to rotations about the x axis, clockwise and counterclockwise, respectively [see Fig. 3(d)]. Comparing Fig. 6(d) with Fig. 4(d), it is clear that even a small tilting angle $\beta=\pi/100$ results in the onset of chaotic motion in the vicinity of the separatrix dividing pendular from free-rotor states.

For collinear fields, $\beta=0$, the (ϕ,p_ϕ) SOS was not shown on account of its trivial structure. Since p_ϕ is a constant of the motion the section $\theta=\theta_0,\dot{\theta}>0$, consists of invariant curves with constant $p_\phi=m$. The invariant line $m=0$ consists of a continuous set of period-1 fixed points. Moreover, the conical stable periodic orbits typically do not appear on the SOS as they have constant $\theta\neq\theta_0$. The (ϕ,p_ϕ) SOS is of greater interest for $\mathcal{A}=1/4$, $\beta\neq 0$. Sections with $\theta=\pi/10$, $\dot{\theta}>0$ are shown in Figs. 7(a) ($\bar{E}=1.0$) and 7(b) ($\bar{E}=0.2$). The line of fixed points with $m=0$ present for $\beta=0$ disappears and is replaced in accord with the Poincaré–Birkhoff theorem by two stable and two unstable fixed points and associated homoclinic tangle.[32] The stable fixed points at $\phi=\pi/2$ and $\phi=3\pi/2$ correspond to the same periodic trajectories associated with the stable fixed points in the $\theta-p_\theta$ surface of section near $\theta=0$ and $\theta=\pi$, respectively (cf. Fig. 6). The unstable fixed points in at $\phi=0$ and $\phi=\pi$ correspond to periodic orbits rotating about the y axis clockwise and counterclockwise, respectively. Details of the sections near $p_\phi\approx 0$ are shown in Figs. 7(c) and 7(d).

2. Larger tilting angles

More complete $\bar{E}$ vs θ plots for periodic orbits on the symmetry line L_S are given in Fig. 8 for $\beta=0$ [Fig. 8(a)], $\beta=0.01\pi$ [Fig. 8(b)], $\beta=0.25\pi$ [Fig. 8(c)], and $\beta=0.5\pi$ [Fig. 8(d)]. These plots are obtained by propagation of points on the symmetry line L_S in Cartesian coordinates, as described in Sec. III A 3. The range of the coordinate θ is formally extended from $0\leqslant\theta\leqslant\pi$ to $0\leqslant\theta\leqslant 2\pi$, where $0\leqslant\theta\leqslant\pi$ for $\phi=0$ and $\pi\leqslant\theta\leqslant 2\pi$ for $\phi=\pi$. An intricate bifurcation structure evolves from the integrable limit. Note that, for $\beta=\pi/2$, the po plots are invariant under the transformations $\theta\rightarrow\pi-\theta$ $(0\leqslant\theta\leqslant\pi)$, and $\theta\rightarrow 3\pi-\theta$ $(\pi\leqslant\theta\leqslant 2\pi)$ induced by the symmetry $\sigma_{xy}:z\rightarrow -z$.

Several (θ,p_θ) SOSs for $\mathcal{A}=1/4$ and $\beta=\pi/4$ are shown for various energies in Fig. 9. At energies well below the barrier height, [$\bar{E}=-0.5$, Fig. 9(f)], the phase space primarily exhibits regular pendular motion, with trajectories confined to one well or the other. At energies well above the barrier height [$\bar{E}=1.5$, Fig. 9(a)], the phase space mainly consists of regular, free-rotor-type motion, although some irregular motion is present near $\theta\approx\pi/2,p_\theta\approx 0$. For energies between these limiting values, the phase space shows large scale chaotic dynamics [Figs. 9(b)–9(e)].

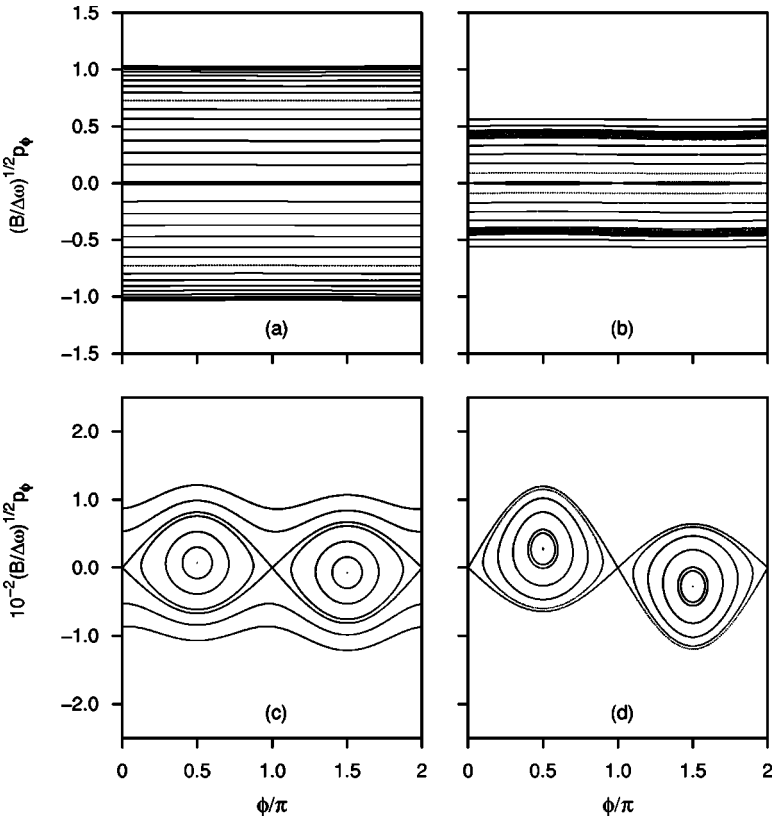

FIG. 7. (ϕ, p_ϕ) surface of section defined by conditions $\theta=\pi/10$, $\dot{\theta}>0$. $\omega/\Delta\omega=1/4$, $\beta=\pi/100$. (a) $\bar{E}=1.0$. (b) $\bar{E}=0.2$. The central resonant chain and two chaotic strips appear. (c) Details of the central resonant chain, $p_\phi \approx 0$, $\bar{E}=1.0$. (d) Details of the central resonant chain, $p_\phi \approx 0$, $\bar{E}=0.2$.

In Sec. V, we examine quantum-mechanical energy-level correlation diagrams and nearest-neighbor level spacing distributions for the parameter values that correspond to the existence of chaotic classical motion.

V. QUANTUM MECHANICS: ENERGY-LEVEL CORRELATION DIAGRAMS AND LEVEL SPACING DISTRIBUTION

A. Energy-level correlation diagrams

Energy-level correlation diagrams (E_n versus Hamiltonian parameter such as the tilting angle or field strength) are important in the study of molecule-field problems. Friedrich and Herschbach have calculated correlation diagrams for low-energy eigenstates of the rotor in parallel fields ($\beta=0$).[25] In Fig. 10(a) we show a correlation diagram for 60 states spanning an energy range from the ground state to well above the barrier for $\omega=60$, $\beta=0$, and $\Delta\omega=150 \rightarrow 300$. At fixed ω, the energies of all eigenstates E_n decrease as $\Delta\omega$ increases, in accord with the Hellmann–Feynman theorem,[68]

$$\frac{\partial E_n}{\partial \Delta\omega} = \langle n|\frac{\partial \hat{H}}{\partial \Delta\omega}|n\rangle = -\langle n|\cos^2\theta|n\rangle. \tag{17}$$

On the other hand, at fixed $\Delta\omega$, energies either increase or decrease as ω increases, depending on the expectation value $\langle n|\partial\hat{H}/\partial\omega|n\rangle = -\langle n|\cos\theta|n\rangle$.

Figure 10(b) is similar to Fig. 10(a), but for tilted fields, $\beta=\pi/4$. Qualitatively, although still monotonically decreasing with $\Delta\omega$, the levels appear to "fan out" more uniformly than in the tilted field case, reflecting increased level repulsion in the nonintegrable case. This qualitative observation is quantified by the computation of nearest-neighbor spacing statistics discussed below.

The existence of extensive avoided crossings in the nonintegrable case is demonstrated more clearly in Fig. 11, which shows a correlation diagram at fixed $\omega=60, \Delta\omega=240$ for the range of tilting angle $\beta=0\rightarrow\pi/2$. The limiting case $\beta=\pi/2$, although nonintegrable, possesses an additional reflection symmetry σ_{xy}, which results in closely spaced pairs of levels.

B. Analysis of nearest-neighbor spacing distributions

Strong state mixing found in systems with no rigorously conserved constants of the motion except the Hamiltonian naturally leads to an association between the existence of extensive avoided crossings and the presence of classical chaos, where trajectories explore all of the available phase spaces.[69–71] The influence of avoided crossings on the quantum level spectrum is quantified by the analysis of the nearest-neighbor spacing (NNS) distribution $P(s)$, where $P(s)ds$ is the probability of the energy difference between two levels lying in the range $s\rightarrow s+ds$. When levels repel each other, $P(s)$ will tend to vanish as $s\rightarrow 0$. Otherwise, $P(s)$ will have its maximum value at $s\sim 0$. Reviews of the basic theory can be found in Refs. 70 and 71.

The analytical form of $P(s)$ is known for ideal limiting cases. When the quantum levels are completely uncorrelated $P(s)=e^{-s}$, the exponential distribution, corresponding to completely regular classical phase space.[72] Strong level repulsion, as found for Hamiltonians with random matrix elements, leads to the Wigner distribution, $P(s)=\pi/2\,se^{-\pi s^2/4}$.[70]

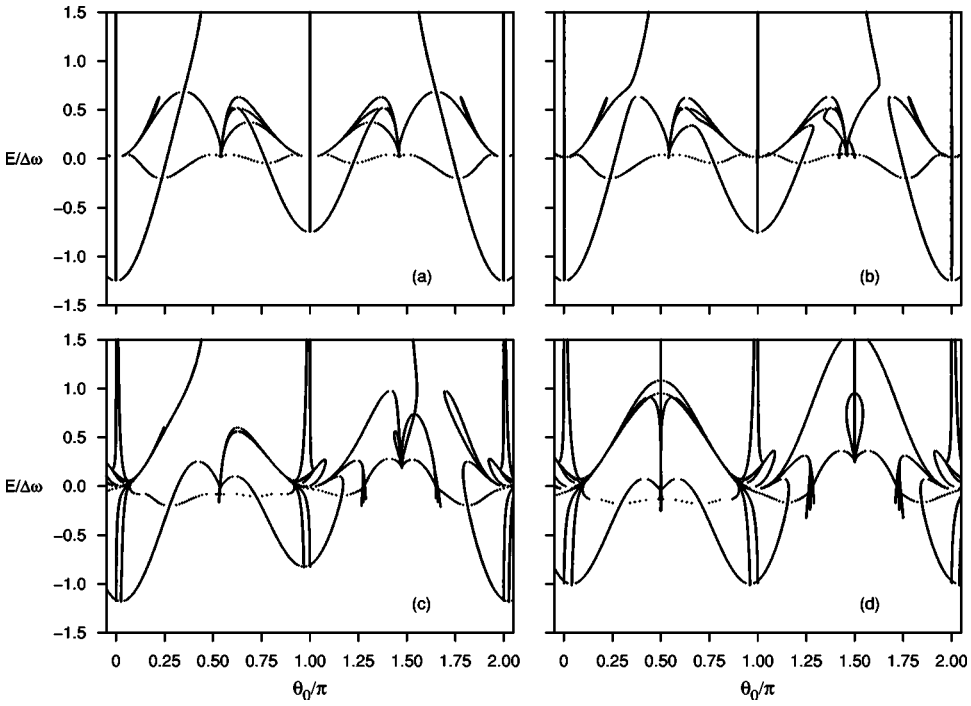

FIG. 8. Energy E vs θ for periodic orbits on symmetry line L_S. Periodic orbits on the symmetry line satisfy either of the conditions $\phi=0$, $\dot{\phi}>0$ or $\phi=\pi$, $\dot{\phi}<0$. $\mathcal{A}=\omega/\Delta\omega=1/4$. (a) $\beta=0$; (b) $\beta=0.01\pi$; (c) $\beta=0.25\pi$; and (d) $\beta=0.5\pi$.

Note that $P(s)\propto s$ at small s. Much numerical evidence supports the notion that level spacings for quantum counterparts of classically strongly chaotic systems are described by the "universal" Wigner distribution.[71]

Classical systems with mixed regular/chaotic phase space fall between these two extremes (for example, Refs. 48 and 73). Calculated level spacing distributions $P(s)$ for such systems can be fitted using one-parameter models that interpolate between the exponential and Wigner distributions, such as the distributions of Berry–Robnik[74] and Brody *et al.*[75] The Berry–Robnik function is a semiclassical result obtained by analyzing the level spacings for a single connected chaotic region in an otherwise regular phase space.[74] A single parameter q, varying between 0 and 1, is the fraction of phase-space volume occupied by the chaotic region. The distribution of Brody *et al.* simply interpolates between exponential and Wigner distributions,

$$P_{\mathrm{Brody}}(s) = (1+q)\beta x^q \exp(-\beta x^{1+q}), \tag{18}$$

where

$$\beta = \left[\Gamma\left(\frac{q+2}{q+1}\right)\right]^{q+1}. \tag{19}$$

The parameter q has no immediate physical interpretation, though it is presumably related to the chaotic phase space

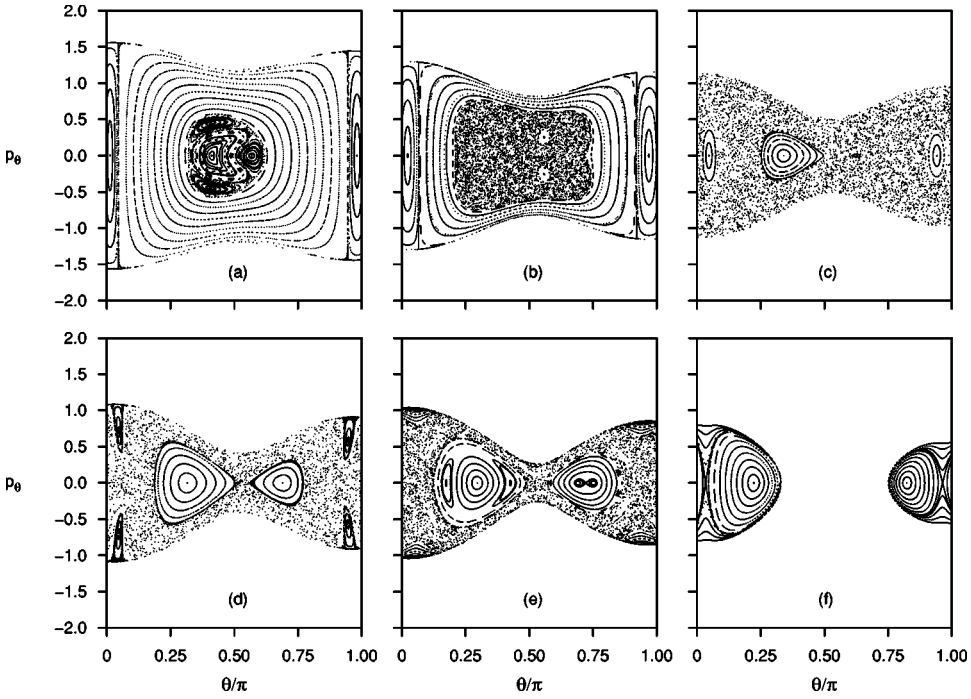

FIG. 9. (θ, p_θ) surfaces of section defined by condition $\phi=0$, $\dot{\phi}>0$. $\mathcal{A}=\omega/\Delta\omega=1/4$, $\beta=\pi/4$. (a) $E=1.5$; (b) $E=1.0$; (c) $E=0.25$; (d) $E=0.1$; (e) $E=-0.1$; and (f) $E=-0.5$.

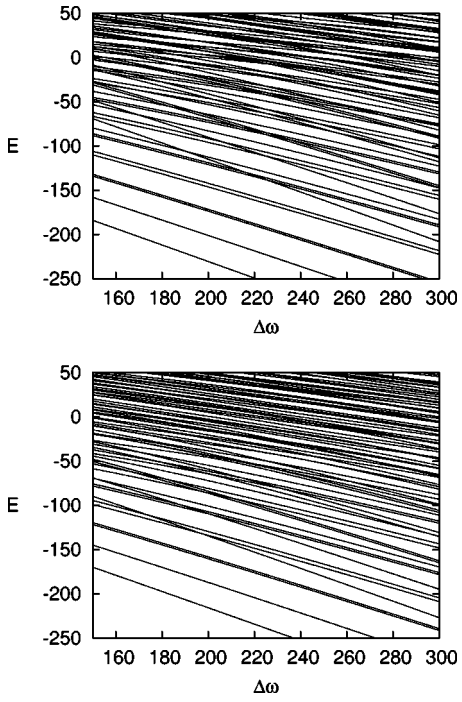

FIG. 10. Energy-level correlation diagram showing lowest 60 energy levels, $\omega=60$, $\Delta\omega=150\rightarrow300$. (a) $\beta=0$. (b) $\beta=\pi/4$.

fraction. Both distributions reduce to the exponential distribution for $q=0$, and to the Wigner distribution for $q=1$.

The standard procedure for calculating $P(s)$ is as follows. First, the calculated or experimental energy-level spectrum is mapped ("unfolded") to a new spectrum with unit mean level density to remove the effect of varying mean level density. The level spacings from the new spectrum are then sorted into histogram bins. This histogram representation of $P(s)$ is then fitted to one of the model distributions, thus determining q. In the calculations reported here we use a fifth-order polynomial to fit the smoothed staircase function $\overline{N}(E)$ (Refs. 70 and 71) and histogram bins with width $\Delta=0.1$.

Several features of the present problem render quantitative analysis of level spacing distributions difficult. Schlier has convincingly demonstrated that q parameters are unreliable when less than several hundred energy levels are used, and recommends using at least a thousand levels.[76] At physically relevant field strengths, our system has less than one hundred bound states in the energy range of interest. Thus we combine smoothed spacings from many independent spectra across a correlation diagram into one histogram.

The tilted fields Hamiltonian (5) has reflection plane symmetry. The existence of a good parity quantum number results in the existence of two uncorrelated level sequences. Only the positive-parity eigenstates are used in our level spacing calculations.

We are particularly interested in learning how changes in classical phase-space structure with energy influence the quantum level spectra. This influence can be monitored by selecting the same N_L levels, from a specified "base state" to the (N_L-1)th level above that, from each spectrum in the correlation diagram as discussed above, and then calculating

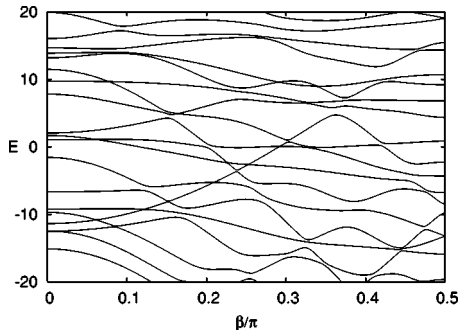

FIG. 11. Energy-level correlation diagram for $\omega=60$, $\Delta\omega=240$, for range of tilt angles $\beta=0\rightarrow\pi/2$.

q. The N_L level window is then moved up to start at the next highest level so that the resulting q corresponds to a slightly higher-energy range. All NNS calculations presented here are of this form.

C. Results for tilted fields

When only one field is on, or the static and laser fields are collinear, the classical problem is integrable with two conserved quantities H and m. In the absence of anomalies such as those associated with, e.g., harmonic-oscillator spectra, $P(s)$ is expected to be exponential, reflecting two interspersed independent spectra creating random spacings.[72,74] Tilting the fields leads to a classically nonintegrable problem and typically mixed phase space. The quantum $P(s)$ exhibits a smaller fraction of spacings in the smallest bins due to more avoided crossings in the correlation diagram, and develops a maximum at $s>0$.

Parameter regimes for NNS calculations must be chosen carefully to obtain meaningful results. We wish to show a correlation between the nature of the classical phase-space structure in a given energy range and the quantum NNS distribution. Lowest-energy states are in the two-dimensional (2D) harmonic-oscillator limit,[43] so including them in the NNS analysis yields anomalous behavior, where $P(s)$ has a maximum near $s=1$ related to harmonic-oscillatorlike states at the bottom of the potential well unrelated to any quantum manifestations of classical chaos.[72] Eigenstates at energies well above the top of the potential-energy barrier are approximately free-rotor eigenstates, and the spectrum at these energies exhibits clusters of almost-degenerate levels. Our analysis is therefore restricted to intermediate energies between these limits.

We have calculated both the parameters of Berry–Robnik.[74] and Brody *et al.*[75] We find that Berry–Robnik q parameters obtained from our analysis are consistently 0.2-0.3 larger than the corresponding q values of Brody *et al.*, but exhibit the same trends. As we are only interested in broad trends rather than quantitative interpretation of the q parameters, we show only the parameters of Brody *et al.* here.

Figure 12 presents plots of the parameter of Brody *et al.* versus base level. The lowest 300 energy levels are analyzed for $\omega=60$, with $\Delta\omega$ in the range of $\Delta\omega=150\rightarrow300$. Figures 12(a)–12(c) show results for tilt angle $\beta=0$, with $N_L=25$ [Fig. 12(a)], 50 [Fig. 12(b)], and 100 [Fig. 12(c)] levels per

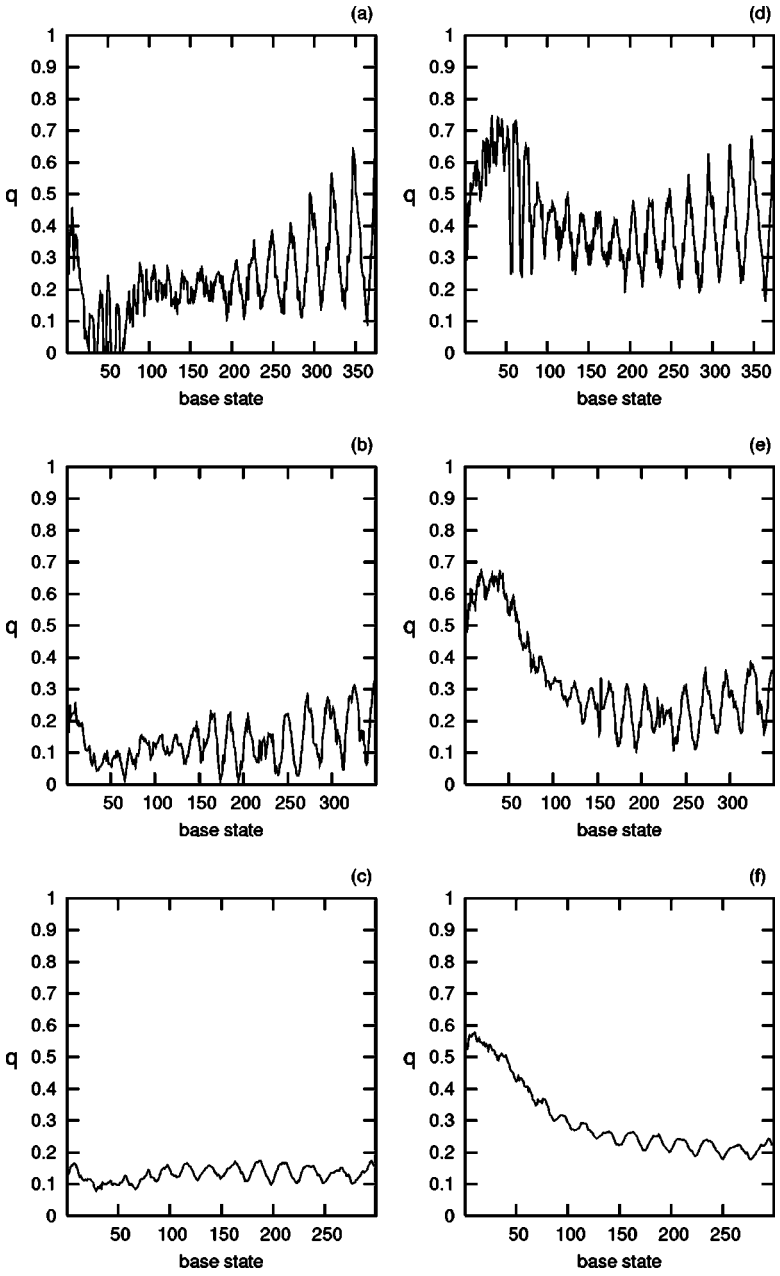

FIG. 12. The parameters of Brody *et al.* extracted from $P(s)$ histograms vs base level. The lowest 300 energy levels are analyzed for $\omega=60$, $\Delta\omega=150\rightarrow300$. (a) Tilt angle $\beta=0$, $N_L=25$ levels per spectrum. (b) $\beta=0$, $N_L=50$. (c) $\beta=0$, $N_L=100$. (d) Tilt angle $\beta=\pi/4$, $N_L=25$ levels per spectrum. (e) $\beta=\pi/4$, $N_L=50$. (f) $\beta=\pi/4$, $N_L=100$.

spectrum, respectively. Figures 12(d)–12(f) show corresponding results for $\beta=\pi/4$. Each data point is calculated from energy levels in the relevant correlation diagram, Fig. 10(a) or 10(b).

Our calculations show that: (i) while there is more "noise" in the $N_L=25$ and $N_L=50$ results, the behavior of q versus state index is consistent for the three N_L values for each value of β; (ii) a clear qualitative difference exists between the energy dependence of q in the integrable ($\beta=0$) and nonintegrable ($\beta=\pi/4$) cases.

Our results are consistent with the underlying classical phase-space structure. The first three panels [Figs. 12(a)–12(c)] show that q is small across the whole energy range, reflecting the regular phase-space structure for collinear fields. The q values obtained for the nonintegrable case $\beta=\pi/4$ first increase then decrease at higher energies, reflecting the change in character of the classical phase space with energy seen in the surfaces of section of Fig. 9. In particular, the transition to regular (free-rotor) behavior at high energies is apparent (cf. Ref. 48). For a nonscaling system with a relatively small density of states, this is about as much information as can meaningfully be extracted concerning NNS distributions.[76]

A similar analysis of NNS distributions for the correlation diagram of Fig. 11 shows that the parameter q of Brody *et al.* is uniformly larger for the spacings at large tilt angles ($\beta=0.3\pi\rightarrow0.4\pi$) compared to those for small tilt angles ($\beta=0\rightarrow0.1\pi$).

Note that the shape of the Berry–Robnik distribution changes most rapidly from exponential to Wigner for q between 0.5 and 1.0, so that the Berry–Robnik distribution with $q=0.5$ is actually very close to an exponential distribution. The distribution of Brody *et al.* (18) changes most rapidly for $0\leqslant q\leqslant0.5$, so the distribution of Brody *et al.* with $q=0.5$ is essentially Wigner-type. Since the collinear field problem is integrable, we should have $q=0$. We attribute discrepancies

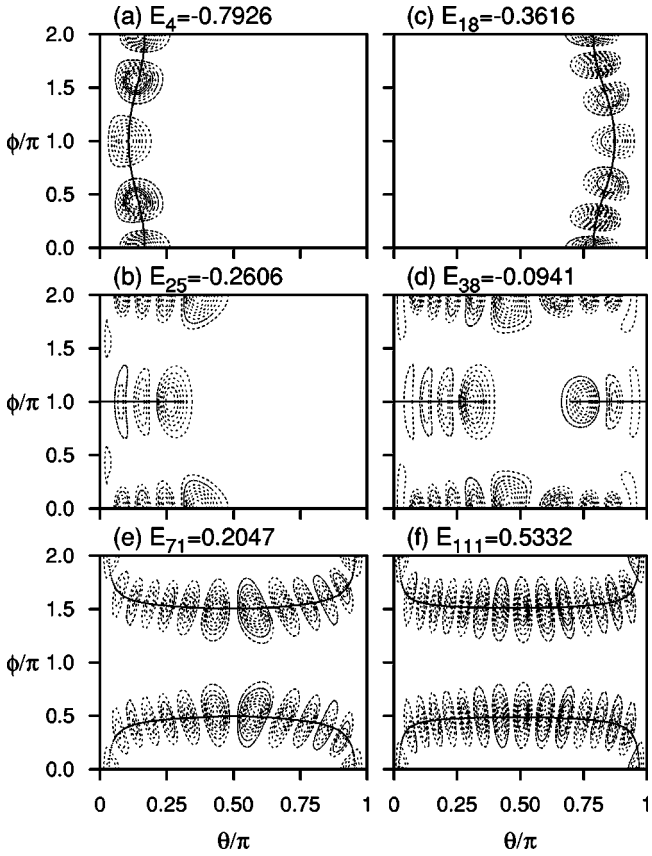

FIG. 13. Probability densities $|\psi(\theta,\phi)|^2 \sin\theta$ for tilted rotor eigenstates $\omega=60$, $\Delta\omega=240$, $\beta=\pi/4$. Scaled eigenvalues are $\tilde{E}=E/\Delta\omega$. Stable classical periodic orbits at the same energy are also shown superimposed on quantum probability densities.

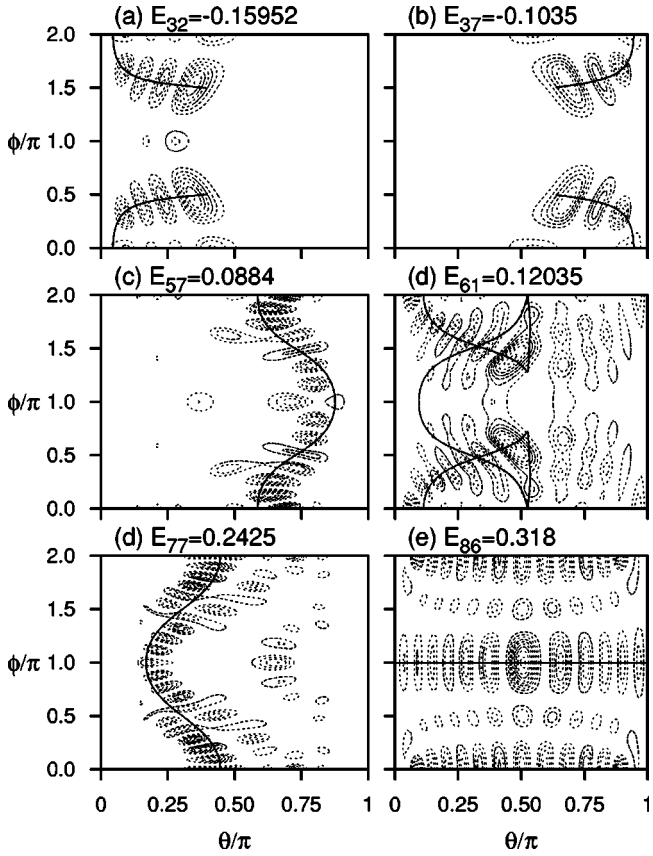

FIG. 14. Probability densities $|\psi(\theta,\phi)|^2 \sin\theta$ for tilted rotor eigenstates. $\omega=60$, $\Delta\omega=240$, $\beta=\pi/4$. Scaled eigenvalues are $\tilde{E}=E/\Delta\omega$. Unstable classical periodic orbits at the same energy are also shown superimposed on quantum probability densities.

between our calculated q values and ideal exponential behavior to the difficulties noted above on the unreliability of q calculations for nonscaling systems with small numbers of levels. For $\beta=\pi/4$, q is well into the Wigner-type region for this nonintegrable problem. As the base level increases, energy increases and q decreases, consistent with increasing regularity of the classical phase space.

VI. QUANTUM MECHANICS: WAVE FUNCTIONS

Energy eigenstates $\psi_\nu(\theta,\phi)$ for the rotor in collinear fields are separable in coordinates θ and ϕ, due to conservation of m. They can, however, exhibit localization in θ (orientation; see Ref. 25).

When the fields are tilted, eigenstates are no longer separable. Examination of rotor eigenfunctions $\psi(\theta,\phi)$ for the tilted field case reveals localization of a significant fraction of rotor eigenstates in the vicinity of classical periodic orbits (see Figs. 13 and 14). These periodic orbits can be stable (cf. Fig. 13), in which case the localized quantum states are associated with a quantizing torus in a regular region of the rotor phase space, or unstable (cf. Fig. 14), in which case we have the phenomenon of scarring.[64] The stable periodic orbits can be those orbits that evolve from the stable relative equilibria in the collinear field case [for example, Figs. 13(a) and 13(c)], leading to states localized in θ, or new stable orbits associated with regular states localized in ϕ [Figs. 13(b) and 13(d)]. Scarring by unstable pos leads to localization in angles θ [Figs. 14(c) and 14(d)], ϕ [Fig. 14(e)], or both [Figs. 14(a), 14(b), and 14(d)].

More definitive characterization of eigenstate localization will require the computation of associated phase-space densities. It is possible to define rotational coherent states, which are parametrized by four classical action-angle variables and are localized in phase space. These states are obtained by suitably modifying the coherent states for diatomic rotors defined by Morales *et al.*,[77] and can be used to define a rotational phase-space density (Husimi function[78]) associated with rotor eigenstates.[63] The rotational Husimi function can then be used to investigate phase-space localization properties of rotor eigenstates.[63]

VII. SUMMARY AND CONCLUSION

In this paper we have investigated the classical and quantum mechanics of diatomic molecules in noncollinear (tilted) static and nonresonant linearly polarized laser fields. The classical diatomic in tilted fields is a nonintegrable system, and we have examined in some detail the phase-space structure for physically relevant parameter regimes for the molecule KCl. While exhibiting low-energy (pendular) and high-energy (free-rotor) limits, the rotor in tilted fields shows chaotic dynamics at intermediate energies in the vicinity of the potential barrier to rotation. The degree of classical chaos

can be tuned by changing the tilt angle, with tilting angles $\simeq \pi/4$ leading to widespread chaos over a wide energy range.

We have examined the quantum mechanics of rotors in tilted fields. Energy-level correlation diagrams have been computed over physically significant ranges of field strengths. Tilting the fields from a collinear configuration leads to the appearance of avoided crossings in the level correlation diagram. The presence of avoided crossings was quantified by the study of nearest-neighbor spacing distributions as a function of energy and tilting angle.

Finally, we examined the influence of classical periodic orbits on rotor wave functions. Many wave functions in the tilted field case are found to be highly nonseparable in spherical polar coordinates (θ, ϕ). Localization of wave functions in the vicinity of classical periodic orbits, both stable and unstable, was observed for many states. Such localization facilitates assignment of the strongly mixed rotor eigenstates obtained with tilted fields.

Nonintegrable dynamics of rotors in various external field configurations provides a rich area for exploration of the classical-quantum correspondence. In model Hamiltonians for molecular vibrational problems, it is found that essential information on the underlying classical mechanics, such as the existence of resonances, is encoded in the level dynamics.[79–82] The same is likely to be true for the problem of rotors in external fields. The connection between phase-space localization and molecule-field level dynamics[83] and the importance of chaotic/dynamical tunneling[84,85] in the tilted strong-field problem are topics deserving further study.

[1] R. J. Gordon and S. A. Rice, Annu. Rev. Phys. Chem. **48**, 601 (1997).
[2] J. P. Simons, Faraday Discuss. **113**, 1 (1999).
[3] R. G. Gordon, L. Zhu, and T. Seideman, Acc. Chem. Res. **32**, 1007 (1999).
[4] P. B. Corkum, C. Ellert, M. Mehendale, P. Dietrich, S. Hankin, S. Aseyev, D. Rayner, and D. Villeneuve, Faraday Discuss. **113**, 47 (1999).
[5] H. Rabitz and W. S. Zhu, Acc. Chem. Res. **33**, 572 (2000).
[6] M. Shapiro and P. Brumer, Adv. At., Mol., Opt. Phys. **42**, 287 (2000).
[7] S. A. Rice and M. Zhao, *Optical Control of Molecular Dynamics* (Wiley, New York, 2000).
[8] M. Shapiro and P. Brumer, *Principles of the Quantum Control of Chemical Reactions* (Wiley-Interscience, New York, 2003).
[9] R. S. Judson, K. K. Lehmann, H. Rabitz, and W. S. Warren, J. Mol. Struct. **223**, 425 (1990).
[10] L. Shen and H. Rabitz, J. Phys. Chem. **95**, 1047 (1991).
[11] R. S. Judson and H. Rabitz, Phys. Rev. Lett. **68**, 1500 (1992).
[12] J. Li, J. T. Bahns, and W. C. Stwalley, J. Chem. Phys. **112**, 6255 (2000).
[13] J. Karczmarek, J. Wright, P. Corkum, and M. Ivanov, Phys. Rev. Lett. **82**, 3420 (1999).
[14] D. M. Villeneuve, S. A. Aseyev, P. Dietrich, M. Spanner, M. Y. Ivanov, and P. B. Corkum, Phys. Rev. Lett. **85**, 542 (2000).
[15] M. Spanner and M. Y. Ivanov, J. Chem. Phys. **114**, 3456 (2001).
[16] M. Spanner, K. M. Davitt, and M. Y. Ivanov, J. Chem. Phys. **115**, 8403 (2001).
[17] R. Hasbani, B. Ostojic, P. R. Bunker, and M. Y. Ivanov, J. Chem. Phys. **116**, 10636 (2002).
[18] R. Blumel, S. Fishman, and U. Smilansky, J. Chem. Phys. **84**, 2604 (1986).
[19] J. Ortigoso, Phys. Rev. A **57**, 4592 (1998).
[20] J. Gong and P. Brumer, J. Chem. Phys. **115**, 3590 (2001).
[21] H. J. Loesch, Annu. Rev. Phys. Chem. **46**, 555 (1995).
[22] A. Auger, A. B. Yedder, E. Cances, C. L. Bris, C. M. Dion, A. Keller, and O. Atabek, Math. Models Meth. Appl. Sci. **12**, 1281 (2002).
[23] H. Stapelfeldt and T. Seideman, Rev. Mod. Phys. **75**, 543 (2003).
[24] B. Friedrich and D. Herschbach, J. Chem. Phys. **111**, 6157 (1999).
[25] B. Friedrich and D. Herschbach, J. Phys. Chem. A **103**, 10280 (1999).
[26] L. Cai, J. Marango, and B. Friedrich, Phys. Rev. Lett. **86**, 775 (2001).
[27] L. Cai and B. Friedrich, in *Laser Control and Manipulations of Molecules*, edited by A. D. Bandrauk, Y. Fujimura, and R. J. Gordon (American chemical society, Washington, DC, 2002), pp. 286–303.
[28] H. Sakai, S. Minemoto, H. Nanjo, H. Tanji, and T. Suzuki, Phys. Rev. Lett. **90**, 083001 (2003).
[29] S. Minemoto, H. Nanjo, H. Tanji, T. Suzuki, and H. Sakai, J. Chem. Phys. **118**, 4052 (2003).
[30] N. H. Nahler, R. Baumfalk, U. Buck, Z. Bihary, R. B. Gerber, and B. Friedrich, J. Chem. Phys. **119**, 224 (2003).
[31] B. Friedrich, N. H. Nahler, and U. Buck, J. Mod. Opt. **50**, 2677 (2003).
[32] A. J. Lichtenberg and M. A. Lieberman, *Regular and Chaotic Dynamics* 2nd ed. (Springer, New York, 1992).
[33] R. H. Cushman and L. M. Bates, *Global Aspects of Classically Integrable Systems* (Birkhauser, Basel, 1997).
[34] M. C. Gutzwiller, *Chaos in Classical and Quantum Mechanics* (Springer, New York, 1990).
[35] I. N. Kozin and R. M. Roberts, J. Chem. Phys. **118**, 10523 (2003).
[36] C. A. Arango, W. W. Kennerly, and G. S. Ezra, Chem. Phys. Lett. **392**, 486 (2004).
[37] R. Cushman and J. J. Duistermaat, Bull. Am. Math. Soc. **19**, 475 (1988).
[38] D. Sadovskii and B. I. Zhilinskii, Phys. Lett. A **256**, 235 (1999).
[39] M. P. Jacobson and M. S. Child, J. Chem. Phys. **114**, 262 (2001).
[40] K. Efstathiou, M. Joyeux, and D. A. Sadovskii, Phys. Rev. A **69**, 032504 (2004).
[41] V. I. Arnold, V. V. Kozlov, and A. I. Neishtadt, *Mathematical Aspects of Classical and Celestial Mechanics* (Springer, New York, 1988).
[42] F. J. Comes, Angew. Chem., Int. Ed. Engl. **31**, 516 (1992).
[43] J. M. Rost, J. C. Griffin, B. Friedrich, and D. R. Herschbach, Phys. Rev. Lett. **68**, 1299 (1992).
[44] B. Friedrich and D. R. Herschbach, Nature (London) **353**, 412 (1991).
[45] B. Friedrich and D. Herschbach, Int. Rev. Phys. Chem. **15**, 325 (1996).
[46] S. C. Ross and K. M. T. Yamada, Mol. Phys. **102**, 1803 (2004).
[47] J. Bulthuis, J. Moller, and H. Loesch, J. Phys. Chem. A **101**, 7684 (1997).
[48] T. P. Grozdanov and R. McCarroll, Z. Phys. D: At., Mol. Clusters **38**, 45 (1996).
[49] B. Friedrich and D. Herschbach, J. Phys. Chem. **99**, 15686 (1995).
[50] J. J. Larsen, H. Sakai, C. P. Safvan, I. Wendt-Larsen, and H. Stapelfeldt, J. Chem. Phys. **111**, 7774 (1999).
[51] B. Friedrich and D. Herschbach, Z. Phys. D: At., Mol. Clusters **36**, 221 (1996).
[52] A. R. Kolovsky, Opt. Commun. **82**, 466 (1991).
[53] J. Ortigoso, M. Rodriguez, M. Gupta, and B. Friedrich, J. Chem. Phys. **110**, 3870 (1999).
[54] R. Escribano, B. Maté, F. Ortigoso, and J. Ortigoso, Phys. Rev. A **62**, 023407 (2000).
[55] M. S. Child, *Semiclassical Mechanics with Molecular Applications* (Oxford University Press, New York, 1991).
[56] P. H. Richter, H. R. Dullin, H. Waalkens, and J. Wiersig, J. Phys. Chem. **100**, 19124 (1996).
[57] M. Joyeux, D. A. Sadovskii, and J. Tennyson, Chem. Phys. Lett. **382**, 439 (2003).
[58] E. Benichou, A. R. Allouche, R. Antoine *et al.*, Eur. Phys. J. D **10**, 233 (2000).
[59] T. C. Bradbury, *Theoretical Mechanics* (Wiley, New York, 1968).
[60] C. W. Gear, SIAM (Soc. Ind. Appl. Math.) J. Numer. Anal. **2**, 69 (1965).
[61] C. A. Arango, Ph.D thesis, Cornell University, 2005.
[62] J. M. Greene, R. S. MacKay, F. Vivaldi, and M. J. Feigenbaum, Physica D **3**, 468 (1981).
[63] W. W. Kennerly, Ph.D. thesis, Cornell University, 2005.
[64] E. J. Heller, Phys. Rev. Lett. **53**, 1515 (1984).
[65] M. P. Jacobson and M. S. Child, J. Phys. Chem. A **105**, 2834 (2001).
[66] J. L. Synge and B. A. Griffith, *Principles of Mechanics unit*, 3rd ed. (Mc-Graw Hill, New York, 1959).
[67] M. Joyeux, S. C. Farantos, and R. Schinke, J. Phys. Chem. A **106**, 5407 (2002).
[68] R. P. Feynman, Phys. Rev. **56**, 340 (1939).
[69] D. W. Noid, M. L. Koszykowski, and R. A. Marcus, Annu. Rev. Phys. Chem. **32**, 267 (1981).
[70] O. Bohigas and M.-J. Giannoni, in *Mathematical and Computational Methods in Nuclear Physics*, Lecture Notes in Physics Vol. 209, edited by J. S. Dehesa, J. M. G. Gomez, and A. Polls (Springer, Berlin, 1984), pp. 1–99.

[71]F. Haake, *Quantum Signatures of Chaos* (Springer, Berlin, 1991).
[72]M. V. Berry and M. Tabor, Proc. R. Soc. London, Ser. A **356**, 375 (1977).
[73]J. Main, M. Schwacke, and G. Wunner, Phys. Rev. A **57**, 1149 (1998).
[74]M. V. Berry and M. Robnik, J. Phys. A **17**, 2413 (1984).
[75]T. A. Brody, J. Flores, J. B. French, P. A. Mello, A. Pandey, and S. S. M. Wong, Rev. Mod. Phys. **53**, 385 (1981).
[76]C. Schlier, J. Chem. Phys. **117**, 3098 (2002).
[77]J. A. Morales, E. Deumens, and Y. Ohrn, J. Math. Phys. **40**, 766 (1999).
[78]K. Takahashi, J. Phys. Soc. Jpn. **55**, 762 (1986).
[79]S. Keshavamurthy, J. Phys. Chem. A **105**, 2668 (2001).
[80]N. R. Cerruti, S. Keshavamurthy, and S. Tomsovic, Phys. Rev. E **68**, 056205 (2003).
[81]A. Semparithi, V. Charulatha, and S. Keshavamurthy, J. Chem. Phys. **118**, 1146 (2003).
[82]A. Semparithi and S. Keshavamurthy, Chem. Phys. Lett. **395**, 327 (2004).
[83]S. Tomsovic, Phys. Rev. Lett. **77**, 4158 (1996).
[84]E. J. Heller, J. Phys. Chem. A **103**, 10433 (1999).
[85]S. Tomsovic and D. Ullmo, Phys. Rev. E **50**, 145 (1994).